scientific reports

Check for updates

OPEN

Assessment of respiratory mechanics and X-ray velocimetry functional imaging in two cystic fibrosis rat models

Nicole Reyne[1,2,3]✉, Ronan Smith[1,2,3], Patricia Cmielewski[1,2,3], Nina Eikelis[4], Mark Lawrence[5], Jennie Louise[6], Piraveen Pirakalathanan[4], David Parsons[1,2,3] & Martin Donnelley[1,2,3]

Two cystic fibrosis (CF) rat models, one carrying the common *Phe508del* mutation and the other a nonsense cystic fibrosis transmembrane conductance regulator (CFTR) mutation (knockout) were previously characterised. Although relevant CFTR mRNA reductions were present in the lung, no overt CF lung disease was observed. This study used flexiVent lung mechanic assessment and regional ventilation assessment via X-ray velocimetry (XV) functional imaging to assess the lung phenotype in both models. To determine the sensitivity of XV regional ventilation imaging, the effect of a localised physical obstruction (delivery of agar beads to part of the lungs) on lung ventilation was examined. At baseline, *Phe508del* and knockout CF rats had a lower inspiratory capacity, total respiratory system compliance, and static compliance than wildtype rats. Following agar bead delivery all XV ventilation parameters were altered, with substantial increases in poorly ventilated regions and ventilation heterogeneity. XV ventilation maps accurately identified locations of bead-induced airflow changes. Despite unremarkable lung histopathology, this study indicated that CF rats display altered respiratory mechanics, with CF rats needing to exert additional effort to expand and deflate their lungs due to increased stiffness. This study demonstrated the utility of XV imaging providing spatial lung ventilation information.

Keywords Cystic fibrosis, Animal models, Lung, Lung function, X-ray velocimetry, flexiVent

Cystic fibrosis (CF) is a life-shortening genetic disease that affects multiple organs[1], but lung disease causes the majority of morbidity and mortality. The CF transmembrane conductance regulator (*CFTR*) is a chloride and bicarbonate ion transport channel on epithelial surfaces that contributes to the absorption and secretion of ions. Pathogenic variants of the *CFTR* gene result in defective CFTR function and altered chloride ion movement, leading to dehydration of the airway surface liquid and impaired mucociliary clearance[2]. Bacteria entering the lungs adhere to the accumulated mucus and are unable to be cleared, resulting in a persistent cycle of infection and inflammation. The combination of mucus stasis, bacterial infections and inflammation contribute to altered lung architecture and airway remodelling, resulting in an obstructive lung disease and progressive decline in lung function. Lung function tests such as spirometry, body plethysmography and multiple breath washout in those with CF are important tools for monitoring pulmonary exacerbation, disease progression and treatment outcomes[3]. In humans these are often combined with lung imaging via computed tomography (CT), or more recently magnetic resonance imaging, to identify structural lung disease including bronchiectasis, mucus plugging, atelectasis, bronchial wall thickening, air trapping and ventilation inhomogeneity[4].

Numerous animal models of CF have been developed, with each displaying a varied CF phenotype[5,6]. Recently, two CF rat models, one carrying the common *Phe508del* mutation and the other a *CFTR* knockout were generated in Adelaide, South Australia[7]. Both models exhibit reduced survival, intestinal obstructions, defects in the male reproductive tract, and a CF bioelectrical profile in the nasal epithelium. However, the classic overt CF muco-obstructive lung disease and histopathology were not observed in either CF rat model, although reduced

[1]Robinson Research Institute, University of Adelaide, Adelaide, SA, Australia. [2]Adelaide Medical School, University of Adelaide, Adelaide, SA, Australia. [3]Respiratory and Sleep Medicine, Women's and Children's Hospital, Adelaide, SA, Australia. [4]4DMedical, Melbourne, VIC, Australia. [5]SCIREQ Scientific Respiratory Equipment Inc, Montreal, QC, Canada. [6]Biostatistics Unit, South Australian Health and Medical Research Institute, Adelaide, SA, Australia. ✉email: nikki.reyne@adelaide.edu.au

CFTR mRNA was present in the lung. McCarron (2020) did not investigate whether lung function differences were present in either of the CF rat models, and this has not been described elsewhere[6].

In research animals the gold standard for measuring airway mechanics is currently the flexiVent small animal ventilator[8]. The flexiVent directly measures pulmonary and airway mechanics by performing a series of forced perturbations and measuring the feedback from the lung. Multiple studies have found that CF mice have an increase in airway resistance, tissue damping, and tissue elasticity when compared to wildtype mice, even in the absence of histopathological findings[9–11]. CF pigs also have similar lung function differences at birth with an increased airway resistance[12]. As with clinical spirometry, although the flexiVent can provide information about lung function, including separation between central and peripheral airways, it cannot spatially localise where within the lung those changes in airflow originate.

X-ray velocimetry (XV) is a new lung imaging technology that is able to provide novel information about lung health[13,14]. When combined with custom XV analysis software, a Permetium preclinical XV scanner (4DMedical, Melbourne, Australia) is able to track the motion of the lung tissue, and display full dynamics of airflow throughout the lung over a breath cycle[15,16]. For laboratory animals, XV ventilation data is acquired using a form of time-resolved CT, in which the volume of multiple (~4000) regions of the lung are tracked throughout the breath. For each region, a parameter called specific ventilation is measured, and is defined as the change in volume of that region relative to the volume of the region at peak exhalation ($\Delta V/V_0$). 3D maps can be used to visualise the specific ventilation data, in the same way absorption values are displayed in traditional CT data.

XV has been applied in animal studies including the β-ENaC mouse model of CF lung disease, to obtain functional information on dynamic airflow and lung function[17,18]. Those studies demonstrated clear differences in the β-ENaC mouse model compared to wildtype littermates, with patchy ventilation corresponding to mucus plugging detected by high-resolution CT and histology. Werdiger et.al provided a quantitative analysis of this[19]. More recently, XV has been used to analyse lobar differences in asthma mouse models[20]. Together these studies suggest XV could be a valuable tool for assessing lung disease in CF rat models[21].

The first aim of this study was to use flexiVent and XV measurements to determine if there are differences in lung function between knockout, *Phe508del* and wildtype rats. The second aim consisted of two parts, firstly to determine if the genotypes would respond differently to an insult from a delivery of agar beads to the lung, and secondly whether XV could detect the location of any airflow defects from this insult.

Methods

Animals

All animal procedures were approved by the South Australia Health and Medical Research Institute (SAHMRI) animal ethics committee under application SAM424.19 and were performed in accordance with the ARRIVE guidelines[22]. Male and female knockout (510X), *Phe508del* and wildtype rats were used (n = 7/group) (Sprague–Dawley background)[7]. Animals were distributed into experimental groups according to genotype, and randomly allocated to receive sterile agar beads (see below) into either their left or right main bronchus. The use of animals of a single sex was not possible due to the challenges associated with breeding large numbers of CF rats. All rats were maintained in conventional cages with a 12-h light/dark cycle. Food and water were provided *ab libitum*, with all rats receiving a 50:50 mix of normal and high fat (10%) rodent chow. CF rats received water containing 4.5% ColonLytely (Dendy Pharmaceuticals, Australia) to minimise CF related gut obstructions. All imaging and lung function tests were performed at the SAHMRI Preclinical Imaging and Research Laboratories (PIRL, South Australia).

X-ray velocimetry (XV)

Rats were anaesthetised with a mixture of 60–75 mg/kg of ketamine (Ceva, Australia) and 0.4–0.5 mg/kg medetomidine (Ilium, Australia), delivered by intraperitoneal injection. Once anaesthetised, the rats were prepared by performing a tracheostomy and cannulation with a cut-down endotracheal tube (ET; 14 Ga BD Insyte plastic cannula bevel cut to 15 mm length), and then restrained in a custom 3D printed holder in an upright position. XV imaging was performed with a Permetium preclinical scanner (4DMedical, Australia), configured with a 1700 mm sample to detector distance. For XV scan acquisition, each rat was placed onto the translation/rotation stage of the Permetium. Animals were connected to a small animal ventilator (4DMedical Accuvent 200, Australia) configured to a peak inspiratory pressure of 14 cmH_2O, positive end-expiratory pressure of 2 cmH_2O, and ventilated at 93.75 breaths/min (192 ms inspiration and 448 ms expiration; I:E ratio of 3:7). A 4D XV scan was then acquired at a framerate of 15.625 Hz, with 10 images per breath and 600 projections per phase-point. The scan time was ~6 min.

In this study, the specific ventilation was only assessed during the inspiratory phase of the breath. Using these X-ray images, specific ventilation values were calculated at ~4000 voxels within the lungs by 4DMedical using their proprietary XV analysis algorithms. From these, the standard parameters of mean specific ventilation (MSV) and ventilation heterogeneity (VH) were calculated. Normalised ventilation defect percentage (nVDP) was calculated using 60% of the MSV of the wildtype group to define a fixed threshold. To explore regional variations, these parameters were also calculated on subsets of the lung volume. Further analysis of the lung volume was done using a custom Python script that bisected the lung into left and right halves. A face-on view was found by rotating the lungs (about the head-to-tail axis) until the separation between the two halves was greatest, bisecting where the lungs were thinnest. The whole-lung metrics defined in Table 1 were used to describe the characteristics of the resulting specific ventilation histogram.

X-ray Velocimetry terminology and metrics		
$\Delta V/V_0$	Specific Ventilation	Inspiration (ΔV) divided by end-expiratory volume (V_0) in the same region. A within-lung dimensionless value
MSV	Mean Specific Ventilation	The mean specific ventilation throughout the whole lung
VDP	Ventilation Defect Percentage	The proportion of the lung with specific ventilation less than 60% of the MSV for that animal
nVDP	Normalised Ventilation Defect Percentage	The proportion of the lung with specific ventilation less than 60% of the MSV of the control population
VH	Ventilation Heterogeneity	Interquartile range divided by the mean specific ventilation. Quantifies the spread of specific ventilation

Table 1. X-ray Velocimetry terminology and metrics.

flexiVent

Immediately following XV imaging, lung function assessments were performed using a flexiVent FX small animal ventilator fitted with a FX4 rat module (SCIREQ, Montreal, Canada) with rats in a supine position. The 14 Ga cannula was connected to the flexiVent and ventilatory parameters set at respiratory rate 90 breaths/min, tidal volume 10 mL/kg and positive end expiratory pressure (PEEP) of 3 cmH_2O. Lung mechanics measurements were made using the SCIREQ automated algorithms configured in a rat mechanics scan script that was repeated three times.

A Deep Inflation manoeuvre maximally inflated the lungs to a pressure of 30 cmH_2O, held over a period of 3 s, to reset lung volume history and measure the inspiratory capacity (IC). A single-frequency (SnapShot-90) perturbation matching the rat respiratory rate and tidal volume, was used to fit the single-compartment model, enabling calculation of the total respiratory system resistance (R_{rs}), compliance (C_{rs}), and elastance (E_{rs}). A broadband (Quick Prime-3) forced oscillation perturbation was then applied, using a range of frequencies above and below the respiratory rate, to which the flexiWare software fit the constant-phase model of respiratory system impedance (Z_{rs}) to calculate Newtonian resistance (R_n), tissue damping (G), and tissue elastance (H). The hysteresivity (Eta) was calculated by dividing G by H. Stepwise pressure-controlled pressure–volume (PVs-P) loops were generated and flexiWare automatically fitted the Salazar-Knowles equation to the expiratory data to obtain an inspiratory capacity estimate (A), curvature of the deflating PV loop (K), and quasi-static compliance (C_{st}). The PV loop area (hysteresis) was also calculated. Data was excluded from any model if the model fit was poor (coefficient of determination less than 0.9). For each parameter, an average of the three measurements was calculated per rat. IC was normalised to body weight.

Sterile agar beads

Sterile agar beads were prepared using previously established methods[23,24], in which 2% molten agar was added to rapidly spinning warmed mineral oil (53 °C) and cooled for 10 min. Agar beads were washed once with 0.5% deoxycholic acid (DCA), once with 0.25% DCA, and three times with phosphate buffered saline, then centrifuged at 1800 RPM for 10 min, with the top layer of oil removed each time. The agar beads (50–100 µm diameter) were resuspended in an equal volume of phosphate buffered saline to form a bead slurry.

Following baseline XV and flexiVent measurements, 50 µl of agar beads were delivered to either the left or right main bronchus by miniature brochscope[25], with rats randomly assigned to each group (either left or right side delivery). Post-bead XV scan and flexiVent measurements were then performed. After all analyses animals were humanely killed by overdose of 150 mg/kg sodium pentobarbital (Lethabarb, Virbac, Australia).

Histology

Lungs were fixed in 10% phosphate-buffered formalin, embedded in paraffin and sectioned at 5 µm. Sections were stained with Haematoxylin and Eosin. Images were examined and captured on a Nikon Eclipse E400 microscope (Tokyo, Japan) with DS-Fi2-U3 camera and Nikon NIS-elements D software version 5.42.08 (Tokyo, Japan).

Statistics

Statistical analyses were performed in R version 4.3.1[26]. ANOVA was used to measure whether age or weight differed substantially at baseline. To assess differences in the flexiVent and XV parameters at baseline between genotypes, and the change from pre- to post-bead delivery within each genotype, a linear mixed effects model was fitted to each parameter using the *lmer* function from the *lme4* package[27]. This model contained fixed effects of genotype, weight, time point, an interaction between genotype and time point, plus a random effect of animal ID. Sex was not included as a variable in the model due to model overfitting. A second model was fitted to assess differences between group parameters after bead delivery, and the potential for effect modification due to the (half) lung into which the beads were delivered. This model contained fixed effects of the baseline parameter value, genotype, the treated lung (left or right), and an interaction between genotype and the treated lung. Pairwise comparisons for each fitted model were performed using the *emmeans* package[28]. Results are presented graphically as estimated marginal means and 95% confidence intervals. Supplementary Table 1 shows the differences in estimated marginal mean between the genotypes and 95% confidence intervals for each parameter, as well as the actual *p* value. Supplementary Table 2 shows the difference in the estimated marginal mean between baseline and post-beads, 95% confidence intervals and the actual *p* value.

Results

Animals

Table 2 shows the characteristics of the three groups. The age distribution was similar between the groups of rats, however the *Phe508del* and knockout rats weighed less on average than the wildtype rats.

Baseline comparison between genotypes

When normalised to body weight, the Deep Inflation manoeuvre showed that wildtype rats had a higher inspiratory capacity IC_{norm} compared to CF rats (Fig. 1A, supplementary Table 1). A single frequency forced oscillation (SnapShot-90) demonstrated total respiratory system compliance C_{rs} was lower in knockout rats compared to wildtype (Fig. 1B). Total respiratory system resistance R_{rs} was not notably different in either CF rat model compared to wildtype (Fig. 1C).

The broadband forced oscillation technique (Quick-Prime 3), which measured Newtonian resistance, tissue damping, elastance, and hysteresivity, showed that there was no substantial difference between wildtype and CF rats at baseline (Supplementary Table 1).

Average pressure volume loops (PVs-P) constructed from mean data showed a downward shift in the *Phe508del* and knockout rats compared to wildtype rats (Fig. 2). The static compliance C_{st}, signifying the intrinsic elastic properties of the lung and chest wall, was lower in *Phe508del* and knockout rats compared to wildtype rats (Fig. 2).

There were no notable differences between the genotypes in any of the XV parameters at baseline (Supplementary Table 1).

Comparison after bead delivery

Figure 3 shows an example of a sterile agar bead obstructing a small airway in the right lower lobe following a bronchoscopic delivery to the right main bronchus.

Post-bead delivery there was a decrease in respiratory system compliance C_{rs} in the wildtype rats compared to baseline. Post-beads there were increases in the tissue damping and tissue hysteresivity in *Phe508del* rats. All

	Wildtype (n = 7)	*Phe508del* (n = 7)	Knockout (n = 7)
Sex	F = 2, M = 5	F = 4, M = 3	F = 6, M = 1
Age (days)	73.7 ± 9.1	75.3 ± 16.8	79.1 ± 16.7
Weight (g)	338 ± 48	243 ± 22 ($p = 0.002$)	196 ± 52 ($p < 0.001$)

Table 2. Rat characteristics. Values are presented as mean ± SD, and differences analysed by ANOVA with post-hoc comparisons to wildtype.

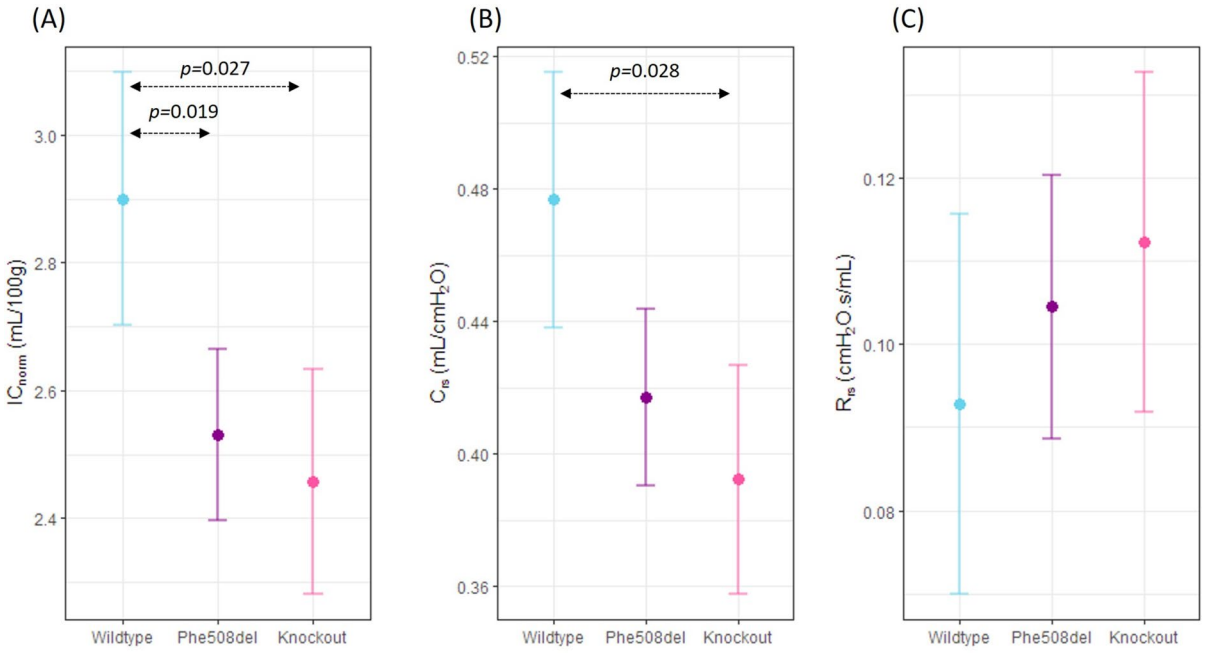

Fig. 1. Respiratory system mechanics in wildtype, *Phe508del* and knockout rats. (**A**) Normalised inspiratory capacity, (**B**) total respiratory system compliance and (**C**) resistance (n = 7 animals/genotype, linear mixed effect model, estimated marginal means and 95% CIs).

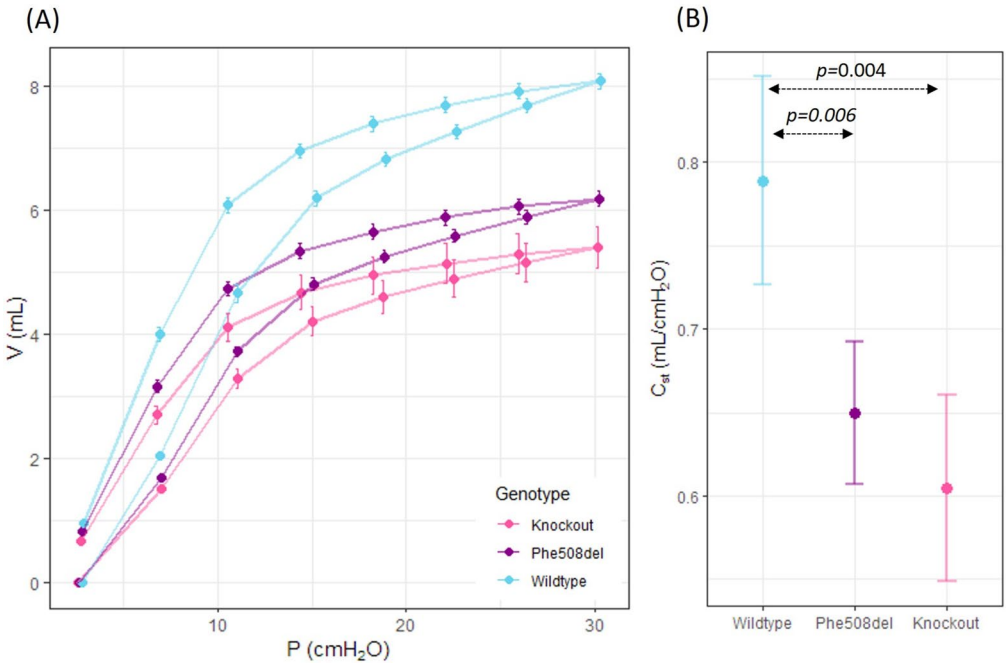

Fig. 2. Pressure–volume loops in wildtype, *Phe508del* and knockout rats. Baseline pressure volume loops were generated using a volume-controlled stepwise manoeuvre (PVs-V) for each genotype. **(A)** Raw pressure volume loops, and **(B)** static compliance (n = 7 animals/genotype, linear mixed effects model, estimated marginal means and 95% CIs).

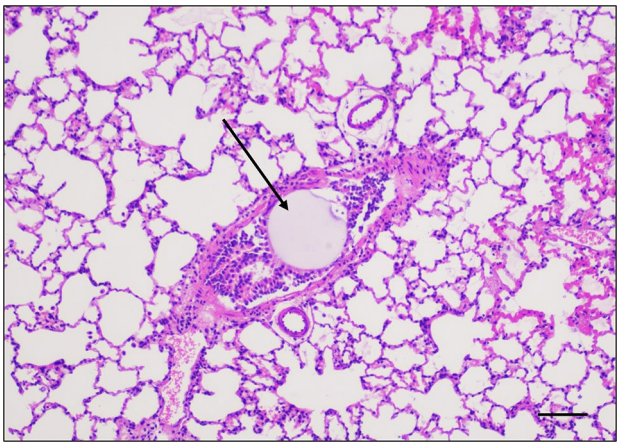

Fig. 3. Representative haematoxylin and eosin image of a sterile agar bead within an airway in the right lower lobe of a rat lung. Scale bar 100 μm.

genotypes had a reduction in the parameter K of Salazar-Knowles equation post-bead delivery, and the PV loop hysteresis was increased in the *Phe508del* and wildtype rats post-beads (supplementary Table 2).

Following delivery of agar beads XV analysis revealed that the MSV was decreased in all genotypes. Normalised VDP and VH were increased in *Phe508del,* and wildtype rats post-bead delivery compared to baseline (Fig. 4).

Examples of ventilation maps at baseline and after agar bead delivery to the lungs are shown in Fig. 5. Differences between the left and right lung were obvious for all animals, with those having right side bead delivery showing reduced ventilation (red) on the corresponding right side, while the left side had areas of higher ventilation (blue). With the exception of MSV, there was no evidence that any of the measures were affected by the choice of lung that received the beads. That is, the differences between genotypes were not affected by whether the right or left lung received the beads.

To quantify regional differences in ventilation, the specific ventilation data for each lung was determined by splitting the whole lung volume into left and right components for analysis. MSV was then calculated in each side of the lung, for the baseline and for the post-bead delivery datasets. The example histograms from two rats

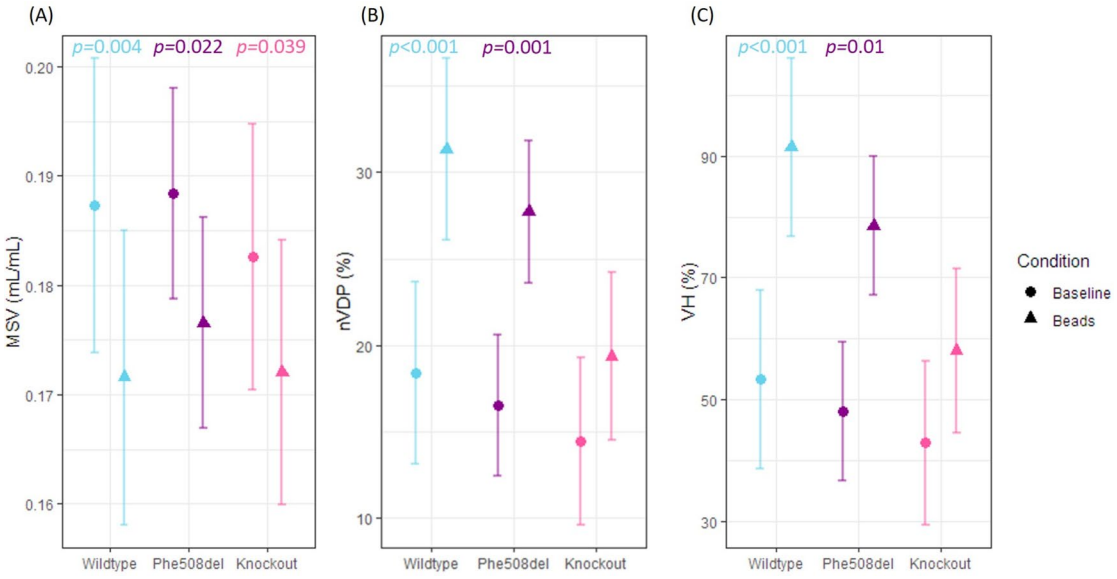

Fig. 4. X-ray Velocimetry parameters at baseline and post-bead delivery in wildtype, *Phe508del* and knockout rats. (**A**) Mean specific ventilation, (**B**) normalised ventilation defect percentage, and **(C)** ventilation heterogeneity. (n = 7 animals/genotype, linear mixed effect model, estimated marginal means and 95% CIs).

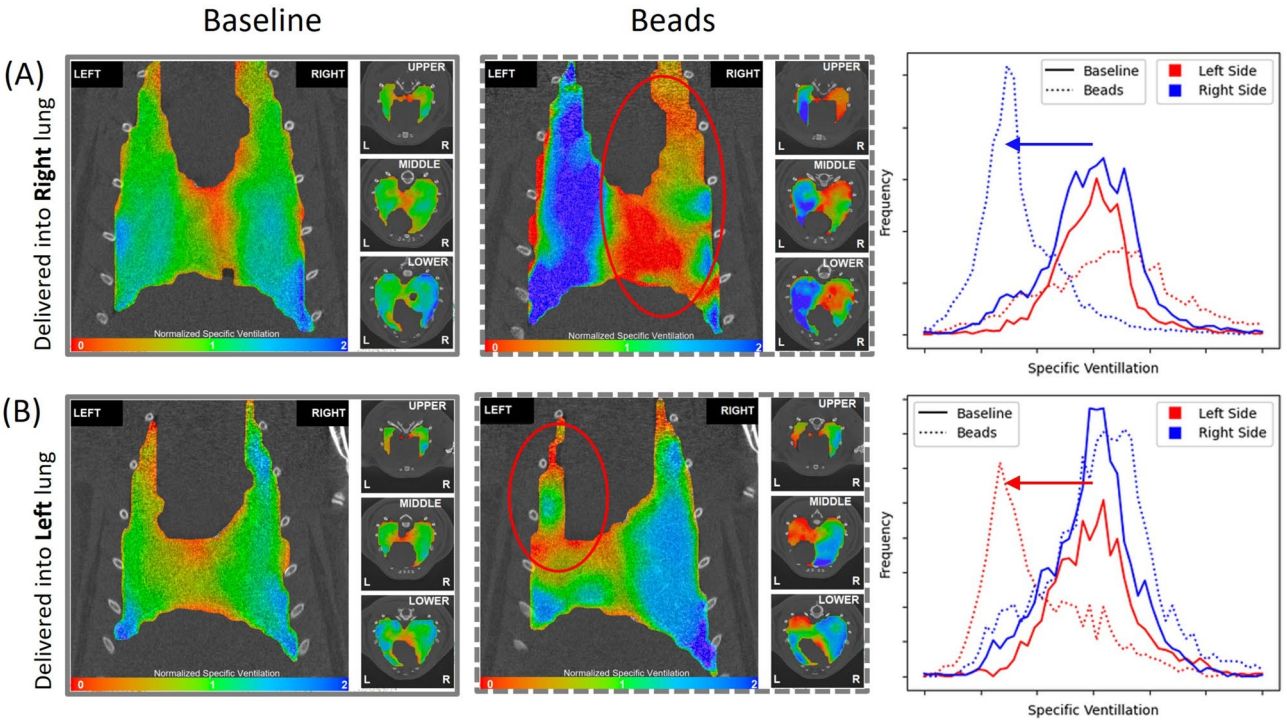

Fig. 5. Visualisation of changes in local ventilation, and frequency distribution of specific ventilation, after agar bead delivery to the lung. (**A**) The top row shows a rat that received agar beads to the right lung, and **(B)** the bottom row shows a rat that received an agar bead delivery to the left lung. Left panel (pre-beads) and middle panel (post-beads): A single mid-coronal slice and three axial slices (upper, middle and lower), showing normalised specific ventilation at peak inspiration. Green indicates average ventilation, red below average ventilation, and blue above average ventilation. Red circle indicates the side beads were delivered to. Right panel: Average histograms of mean specific ventilation in right (blue) and left (red) lungs pre- (solid line) and post-bead (dot line) delivery in rats.

shown in Fig. 5 (right panel), indicate that the left and right lung had a similar specific ventilation distribution prior to delivery. However, once the beads were delivered, the MSV decreased in the lung that received beads.

Figure 6 shows how the MSV value of each lung in every animal changed after the beads were delivered. The background of the plot is coloured, with the light-red zone showing animals in which the MSV was decreased in both lungs, the yellow zone where one lung had decreased MSV and the other had an increased MSV (i.e. the lung displays compensation), and the green zone where both lungs had an increased MSV. The intersection point indicates the point of no MSV change; the rat at this point exhibits what we consider to be a normal untreated-animal ventilation map, showing mostly green level ventilation, with some red (low ventilation) around the heart. Most rats reside in the yellow zone, indicating that the MSV decreased in one lung, and increased in the other. The rats that had ventilation changes in the light-red and green zones were all close to the intersection point,

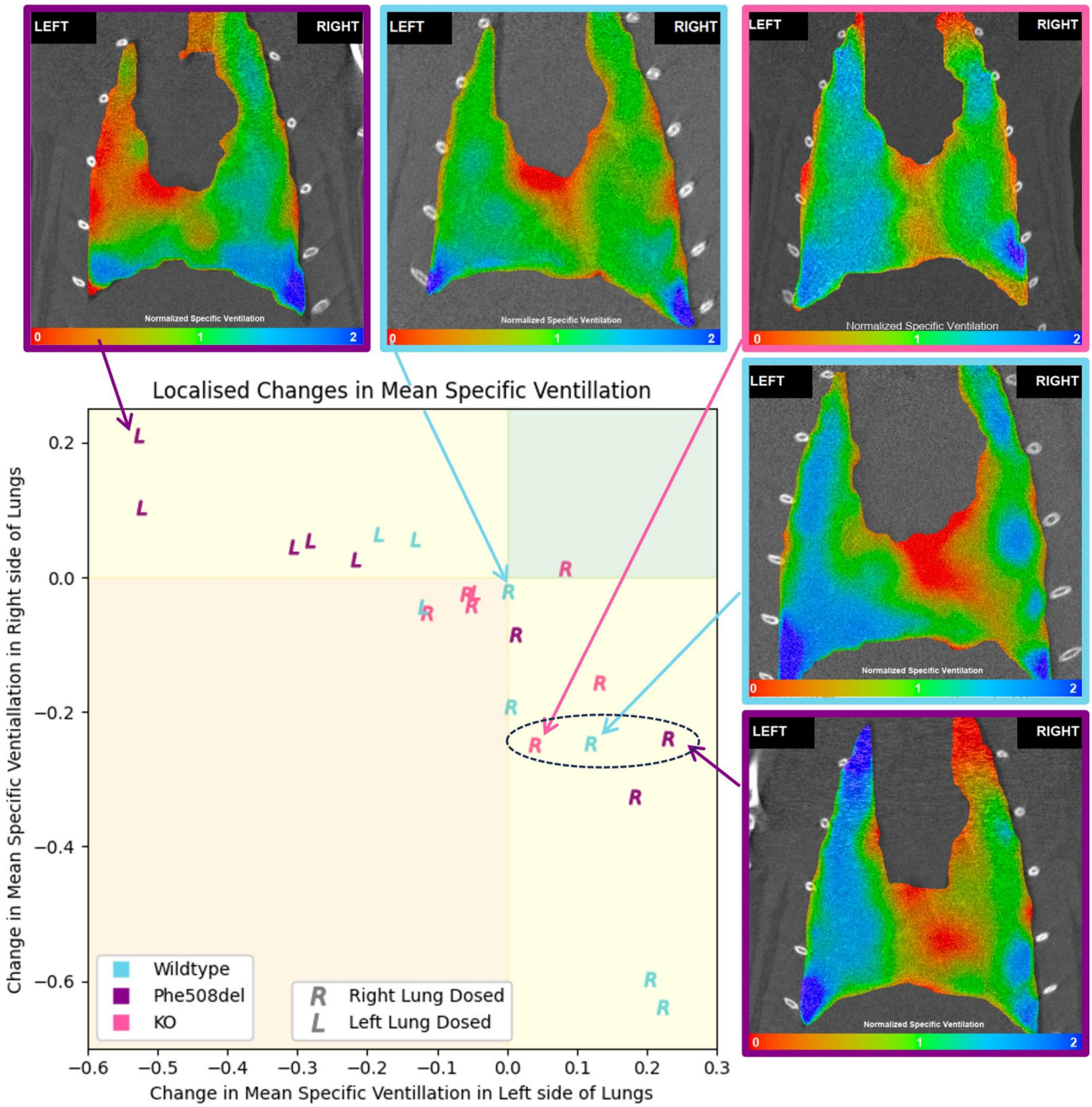

Fig. 6. Localised changes in ventilation can be visualised and quantified. A single mid-coronal slice from different rats showing different areas of ventilation depending on where the bead delivery occurred. Red zones indicate below average ventilation, blue above average ventilation, and green average ventilation. Each rat is marked with the letter L or R to indicate which lung received the bead dose and is coloured by genotype. These five rats were selected to show the different maps that result from animals in different locations on the plane.

indicating that their specific ventilation changes were comparatively small. The group of animals circled show how the changes in right-side MSV could vary, while the changes in left-side MSV remained relatively constant.

Discussion

In human CF lung disease, a significant clinical feature is the progressive decline in lung function. Pulmonary function tests serve as essential tools for tracking lung disease progression in CF, as well as describing the respiratory system characteristics. Animal models of CF are invaluable for investigating disease pathogenesis and conducting treatment development studies. While several animal models of CF have been developed, many of them do not replicate the lung phenotype observed in people with CF[5]. The present study extends our original characterisation of two CF rat models, and we demonstrate for the first time that CF rats have altered respiratory mechanics, even in the absence of histopathological evidence of lung disease[7]. In that characterisation, the *Phe508del* rat typically had an intermediate phenotype for the parameters we reported. In the present study, the *Phe508del* rat also exhibited an intermediate lung phenotype compared to the knockout and wildtype rats[7].

The flexiVent assessments identified differences in the lung function of CF rats at baseline. We chose to age-match rather than weight-match the rats in our study design. Weight matching would have necessitated the use of younger wildtype rats, potentially introducing additional variables due to the immaturity of their respiratory system. By not weight-matching, we ensured that the CF rats were comparable to wildtypes in their age-appropriate characteristics, allowing us to evaluate the impact of the CF genotype on lung function, and as a result the CF rats were smaller than the wildtype rats.

Single frequency forced-oscillation assessment (Single Compartment Model) provides a comprehensive evaluation of the resistive and elastic properties of the respiratory system, encompassing the lungs, chest wall and airways. At baseline, knockout CF rats exhibit lower dynamic compliance compared to wildtype rats, suggesting that CF rats have stiffer lungs. Pressure-driven pressure volume loops were used to further assess the compliance of the respiratory system across the entire inspiratory capacity. When performed at baseline, CF rats also exhibited reduced static compliance, indicating a respiratory system (comprising the lung and chest wall) that is less distensible. This observation aligns with the outcomes obtained from the forced-oscillation analysis.

Comparable lung function outcomes were observed using the flexiVent system in two separate studies involving CF mice[9] and a mouse model of fibrosis[29]. In the study conducted by Darrah (2016), two different CF mouse models were characterised against their littermate wildtypes[9]. Significant changes in resistance between central and peripheral airways were reported, with the peripheral airways being the primary source of increased resistance in CF mice due to the decreased static compliance[9]. Furthermore, this model confirmed an enlargement of the distal airspaces as the anatomical basis for changes in pulmonary mechanics. These studies collectively highlight the effectiveness of the flexiVent system as a valuable tool for assessing lung function in rodent models. Nevertheless, the parameterized lung mechanics of the flexiVent do not allow for spatial mapping of changes that may be these localised alterations in airflow, especially where unaffected lung areas compensate for the affected regions[8].

The second aim was to investigate the impact of a single-lung insult on the lung parameters measured by the flexiVent and XV systems, and in particular if these obstructive effects could be localised to the locations where beads were delivered. The agar beads were delivered to either the right or left main bronchus after the baseline measurements were performed. The pressure volume loop parameters were altered, with changes in the area and shape of the curve observed. However, the flexiVent is unable to spatially determine the location within the lung where the agar beads were delivered.

XV ventilation analysis provided a wealth of information about the lung post bead delivery. All XV parameters in the wildtype and *Phe508del* rats were altered post-bead delivery. Interestingly, the knockout rats unexpectedly observed no difference post-bead delivery. Most importantly, changes in ventilation post-bead delivery clearly could be visualised in the ventilation maps. While this study only presented 2D representations of XV data, it is important to note that XV data can be visualised in 4D format (3D plus time), which could provide even more detailed insights to ventilation.

To delve deeper into the changes of the ventilation, the raw data from specific ventilation across the lung was divided into left and right lung components. We then compared the pre- and post-bead delivery histograms of the right and left lungs, revealing changes in ventilation on both sides that were consistent with how targeted bead obstructions would be predicted to affect lung ventilation. These changes were quantified and visualised and showed that the specific ventilation of each rat was affected differently by the same delivery of beads to the lung. Future studies should examine whether this type of approach can be used to quantify obstruction severity.

Lung function measurements play a crucial role in diagnosing, monitoring, and assessing outcomes in CF. The current gold standard in human lung function assessment is spirometry, which measures dynamic volumes and capacities during forced expiration and inspiration. It provides essential data such as forced expiratory volume in one second (FEV_1) and forced vital capacity (FVC) in older children and adults. However, spirometry has its limitations. As a global measure, it may lack sensitivity in detecting small changes and might not always offer valuable diagnostics information, or target treatments. In CF, the lung disease can be heterogeneous, and these measurements are unable to capture detail of within-lung variability. Additionally, spirometry requires effort-dependent cooperation, making it unsuitable for children under the age of six. Recent studies have validated the use of XV in a cohort of non-lung cancer patients[30], and healthy volunteers[31], and was shown to produce repeatable and quantitative regional ventilation data. The next key step is to assess XV utility as a monitoring tool in paediatric CF patients[32]. This could transform CF care by offering a more detailed, less effort-dependent method for monitoring lung function and tailoring treatments.

In conclusion, the present study is the first to demonstrate lung function differences in CF rat models, using the flexiVent and XV imaging. Further, in determining the effect of an obstruction on the lung, XV also provided information about the location effect of those airway obstructions.

Data availability

The data can be found at https://doi.org/10.25909/25734549.

Received: 6 June 2024; Accepted: 28 August 2024
Published online: 17 September 2024

References

1. Vallières, E. & Elborn, J. S. Cystic fibrosis gene mutations: Evaluation and assessment of disease severity. *Adv. Genomics Genet.* **4**, 161 (2014).
2. Malhotra, S., Hayes, D. Jr. & Wozniak, D. J. Cystic fibrosis and pseudomonas aeruginosa: The host-microbe interface. *Clin. Microbiol. Rev.* **32**(3), 10–128 (2019).
3. Kołodziej, M. *et al.* Lung function imaging methods in cystic fibrosis pulmonary disease. *Respir. Res.* **18**, 1–11 (2017).
4. Ramsey, K. A. *et al.* Lung clearance index and structural lung disease on computed tomography in early cystic fibrosis. *Am. J. Respir. Crit. Care Med.* **193**(1), 60–67 (2016).
5. McCarron, A., Donnelley, M. & Parsons, D. Airway disease phenotypes in animal models of cystic fibrosis. *Respir. Res.* **19**(1), 54 (2018).
6. McCarron, A., Parsons, D. & Donnelley, M. Animal and cell culture models for cystic fibrosis: Which model is right for your application?. *Am. J. Pathol.* **191**, 228–242 (2020).
7. McCarron, A. *et al.* Phenotypic characterization and comparison of cystic fibrosis Rat models generated using CRISPR/Cas9 gene editing. *Am. J. Pathol.* **190**(5), 977–993 (2020).
8. Ahookhosh, K., Vanoirbeek, J. & Vande Velde, G. Lung function measurements in preclinical research: What has been done and where is it headed?. *Front. Physiol.* **14**, 1130096 (2023).
9. Darrah, R. J. *et al.* Early pulmonary disease manifestations in cystic fibrosis mice. *J. Cyst. Fibros.* **15**(6), 736–744 (2016).
10. Craig Cohen, J. *et al.* The "Goldilocks Effect" in Cystic Fibrosis: Identification of a lung phenotype in the cftr knockout and heterozygous mouse. *BMC Genet.* **5**(1), 21 (2004).
11. Haque, A. *et al.* Chemically modified hCFTR mRNAs recuperate lung function in a mouse model of cystic fibrosis. *Sci. Rep.* **8**(1), 1–14 (2018).
12. Adam, R. J. *et al.* Air trapping and airflow obstruction in newborn cystic fibrosis piglets. *Am. J. Respir. Crit. Care Med.* **188**(12), 1434–1441 (2013).
13. Vliegenthart, R. *et al.* Innovations in thoracic imaging: CT, radiomics, AI and x-ray velocimetry. *Respirology* **27**(10), 818–833 (2022).
14. Parsons, D. & Donnelley, M. Will airway gene therapy for cystic fibrosis improve lung function? New imaging technologies can help us find out. *Hum. Gene Ther.* **31**(17–18), 973–984 (2020).
15. Dubsky, S. *et al.* Synchrotron-based dynamic computed tomography of tissue motion for regional lung function measurement. *J. R. Soc. Interface* **9**(74), 2213–2224 (2012).
16. Fouras, A. *et al.* Altered lung motion is a sensitive indicator of regional lung disease. *Ann. Biomed. Eng.* **40**(5), 1160–1169 (2012).
17. Murrie, R. P. *et al.* Real-time in vivo imaging of regional lung function in a mouse model of cystic fibrosis on a laboratory X-ray source. *Sci. Rep.* **10**(1), 1–8 (2020).
18. Stahr, C. S. *et al.* Quantification of heterogeneity in lung disease with image-based pulmonary function testing. *Sci. Rep.* **6**(1), 29438 (2016).
19. Werdiger, F. *et al.* Quantification of muco-obstructive lung disease variability in mice via laboratory X-ray velocimetry. *Sci. Rep.* **10**(1), 1–12 (2020).
20. Asosingh, K. *et al.* Preclinical four-dimensional functional lung imaging and quantification of regional airflow: A new standard in lung function evaluation in murine models. *Am. J. Respir. Cell Mol. Biol.* **67**(4), 423–429 (2022).
21. Reyne, N. *et al.* Effect of elexacaftor-tezacaftor-ivacaftor on nasal potential difference and lung function in Phe508del rats. *Front. Pharmacol.* **15**, 1362325 (2024).
22. Percie du Sert, N. *et al.* The ARRIVE guidelines 2.0: Updated guidelines for reporting animal research*. *J. Cereb. Blood Flow Metab.* **40**(9), 1769–1777 (2020).
23. Henderson, A. G., et al., Static mucus impairs bacterial clearance and allows chronic infection with Pseudomonas aeruginosa in the cystic fibrosis rat. Eur. Respir. J. (2022).
24. van Heeckeren, A. M. & Schluchter, M. Murine models of chronic Pseudomonas aeruginosa lung infection. *Lab. Anim.* **36**(3), 291–312 (2002).
25. McIntyre, C. *et al.* Lobe-specific gene vector delivery to rat lungs using a miniature bronchoscope. *Hum. Gene Ther. Methods* **29**(5), 228–235 (2018).
26. R Core Team, *R: A Language and Environment for Statistical Computing*. 2022, R Foundation for Statistical Computing.
27. Bates, D. *et al.* Fitting linear mixed-effects models using lme4. *J. Stat. Softw.* **67**(1), 1–48 (2015).
28. Lenth, R.V., *emmeans: Estimated Marginal Means, aka Least-Squares Means*. 2022.
29. Devos, F. C. *et al.* Forced expiration measurements in mouse models of obstructive and restrictive lung diseases. *Respir. Res.* **18**(1), 123 (2017).
30. Kirkness, J. P. *et al.* Association of x-ray velocimetry (XV) ventilation analysis compared to spirometry. *Front. Med. Technol.* **5**, 1148310 (2023).
31. Siddharthan, T. *et al.* Quantifying ventilation by X-ray velocimetry in healthy adults. *Respir. Res.* **24**(1), 215 (2023).
32. Matthew, B. *et al.* Pilot study of paediatric regional lung function assessment via X-ray velocimetry (XV) imaging in children with normal lungs and in children with cystic fibrosis. *BMJ Open* **14**(2), e080034 (2024).

Acknowledgements

The authors acknowledge the facilities and scientific and technical assistance of the National Imaging Facility, a National Collaborative Research Infrastructure Strategy (NCRIS) capability, at the Large Animal Research and Imaging Facility, South Australian Health and Medical Research Institute. The authors acknowledge Wick Lakshantha and Ryan O'Hare Doig for operating the Permetium small animal scanner. This project built on experiments M11727, M12061 and M12926 performed on the Imaging and Medical Beamline at the Australian Synchrotron, and the authors thank Kaye Morgan, Marcus Kitchen, and Bernadette Boog for their input.

Author contributions

N.R.: Conceptualisation, Data Curation, Formal analysis, Investigation, Methodology, Visualization, Writing—Original Draft. R.S.: Data Curation, Formal analysis, Investigation, Software, Visualization, Writing—Original Draft. P.C.: Investigation, Methodology, Data curation, Writing—Review and Editing. J.L., M.L., N.E., P.P.: Formal analysis, Writing – Review & Editing. D.P.: Conceptualisation, Formal analysis, Resources, Methodology, Supervision, Writing—Original Draft, Writing—Review and Editing. M.D.: Conceptualisation, Data Curation, Formal analysis, Funding acquisition, Investigation, Methodology, Supervision, Visualization, Writing—Original Draft.

Funding

Studies were supported by NHMRC Project Grant GNT1160011, Cystic Fibrosis Foundation Grant DONNEL21GO, and the Medical Research Future Fund Grant RFRHPSI000013.

Competing interests

MD and DP were involved in the research development and validation of the XV technology and have personally purchased shares in 4DMedical. NE and PP are employed by 4DMedical. ML is employed by SCIREQ Scientific Respiratory Equipment Inc.

Additional information

Supplementary Information The online version contains supplementary material available at https://doi.org/10.1038/s41598-024-71632-8.

Correspondence and requests for materials should be addressed to N.R.